



# Retrieving stratospheric ozone profiles from OMPS limb profiler measurements

Fang Zhu<sup>1</sup>, Xiaoping Liu<sup>1</sup>, Suwen Li<sup>1</sup>, and Fuqi Si<sup>2</sup>

<sup>1</sup>Anhui Province Key Laboratory of Pollutant Sensitive Materials and Environmental Remediation, Anhui Province Key Laboratory of Intelligent Computing and Applications, School of Physics and Electrical Information, Huaibei Normal University, Huaibei, 235000, Anhui, China

<sup>2</sup>Centre of Environmental Optics, Anhui Institute of Optics and Fine Mechanics, Hefei Institutes of Physical Science, Chinese Academy of Sciences, Hefei, Anhui 230031, China

**Correspondence:** Fang Zhu (zhufang160@163.com)

Received: 11 November 2025 – Discussion started: 1 December 2025

Revised: 21 May 2026 – Accepted: 1 June 2026 – Published: 6 July 2026

**Abstract.** This study presents an independent retrieval algorithm combining wavelength pairing and the multiplicative algebraic reconstruction technique (MART) to process Ozone Mapping and Profiler Suite (OMPS) limb observations for vertical ozone profiles. Developed as a complementary dataset for validating operational products, the algorithm is tailored to OMPS limb profiler's specific characteristics. The retrieval algorithm employs scattered solar radiance measurements from the OMPS/LP, focusing on the visible spectral range, normalizes this radiance to that at an upper tangent height, and retrieves ozone concentrations between 12–40 km. Additionally, it enables the identification of cloud-contaminated measurements at specific altitudes within the instrument field of view. A comprehensive error analysis reveals that prior uncertainty contributes  $\sim 5\%$  error in the tropical lower stratosphere (based on a  $+5\%$  perturbation experiment), while a 30% uncertainty in the aerosol extinction coefficient causes  $\sim 5\%$  error at 15–25 km. Absorption cross-section uncertainties introduce localized biases of  $-3\%$  to  $-5\%$ , and random measurement noise exhibits strong altitude dependence, with values below 10% in the mid-stratosphere and exceeding 20% at high altitudes and in the tropical upper troposphere. OMPS data spanning the entire year of 2021 are processed, and the results are evaluated through comparisons with multiple independent datasets, including NASA official products, passive satellite observations, and in-situ measurements from balloon-borne ozonesondes. At 17–36 km, deviations from OMPS/LP v2.6 data are  $\leq 5\%$ ; at 18–35 km, consistency with Microwave

Limb Sounder (MLS) v5.0 data ranges from 5%–10%; at 20–35 km, most deviations from OSIRIS v7.3 data are  $\leq 5\%$  (except near 23 km). Comparisons with ozonesonde measurements reveal that differences in the 13–30 km range over northern mid-to-high latitudes are mostly  $< 10\%$  (with 10%–15% differences at 22–25 km in polar regions). Over southern mid-latitudes, the consistency within the same altitude range is 2%–10%. Notably, deviations between the retrieved profiles and comparison products increase significantly in the tropics at low altitudes.

## 1 Introduction

Stratospheric ozone forms a natural barrier protecting life on Earth by absorbing solar ultraviolet (UV) radiation. Additionally, as a key greenhouse gas, it participates in the absorption and emission of infrared radiation in the stratosphere, playing a crucial role in regulating Earth's energy balance and stabilizing the climate system (Li et al., 2023a). Dynamic changes in stratospheric ozone concentrations not only directly reflect the emission fluxes and chemical reaction processes of various atmospheric substances, but also serve as an important indicator for assessing the impact of human activities on the atmospheric environment (Young et al., 2021; Chipperfield and Bekki, 2024). Since the identification of the Antarctic ozone hole in the 1980s, research on the evolution patterns and driving mechanisms of stratospheric ozone concentration has remained a core topic in atmospheric science,

attracting global research efforts to continuously explore its variation mechanisms and ecological effects.

High-precision retrieval of stratospheric ozone vertical profiles is a core requirement for advancing stratospheric ozone research and establishing long-term essential climate variable datasets (Jia et al., 2015). To this end, multi-platform monitoring technologies – including ground-based, balloon-borne, airborne, and satellite-based instruments – have been widely applied over recent decades. Among these, satellite observations are categorized by detection modes into nadir, occultation, and limb observations. Nadir-viewing instruments, which observe downward, offer excellent horizontal coverage, with typical examples including the Ozone Monitoring Suite–Nadir (OMS-N) aboard Fengyun-3F (Zhu et al., 2025b), the Ozone Monitoring Instrument (OMI) aboard Aura (Veefkind et al., 2006), and the Environmental Monitoring Instrument (EMI) onboard the hyperspectral observation satellite GeoFen-5 (Qian et al., 2024). Occultation instruments, which directly view the solar disk, are represented by the Stratospheric Aerosol and Gas Experiment (SAGE III) (Cisewski et al., 2014), Atmospheric Chemistry Experiment (ACE) (Bernath et al., 2005), and Global Ozone Monitoring by Occultation of Stars (GOMOS) (Bertaux et al., 2010), featuring high vertical resolution and good signal-to-noise ratio. Limb scattering/emission observations combine the advantages of the aforementioned two modes, boasting high sensitivity, favorable vertical resolution, and high spatial sampling rates, such as the Microwave Limb Sounder (MLS) (Waters et al., 2006), SCanning Imaging Absorption spectroMeter for Atmospheric Cartography (SCIAMACHY) (Burrows et al., 1995), and Optical Spectrograph and InfraRed Imager System (OSIRIS) (Llewellyn et al., 2004). The Ozone Mapping and Profiler Suite (OMPS), a passive imaging spectrometer employed in this study, is onboard the Suomi-National Polar-orbiting Partnership (SNPP) satellite (Flynn et al. 2014). Its limb profiler (OMPS/LP) enables accurate retrieval of stratospheric ozone vertical profiles via limb observation mode. Since 2012, the NASA team has successively developed and released four versions of the ozone LP retrieval algorithm for OMPS limb observation data (the first version was released (Rault et al., 2013), the second version in 2014 (Xu et al., 2014), version 2.5 in 2017 (DeLand et al., 2017), and version 2.6 in 2023 (Kramarova, 2023)). The University of Bremen has also applied its self-developed retrieval algorithm to OMPS/LP measurements (Arosio et al., 2018). In addition, another approach to processing OMPS/LP data employs a 2-D geometry retrieval method, as demonstrated in the work conducted at the University of Saskatchewan (Zawada et al., 2018).

This study focuses on ozone profile retrieval from OMPS/LP observation data, employing a retrieval algorithm based on wavelength pairing and the multiplicative algebraic reconstruction technique (MART). The algorithm is derived from the OSIRIS ozone profile retrieval scheme developed by the University of Saskatchewan. While the core retrieval

methodology of wavelength pairing and MART is well-established in limb sounding, the novelty of this work lies in its tailored adaptation to the OMPS/LP instrument. Given the significant differences between OMPS/LP and OSIRIS in measurement technologies – including spectral resolution, spectral channels, wavelength range, atmospheric sampling, and radiance acquisition – this study has performed targeted optimizations and innovations on the algorithm. These include significant adaptations in radiative transfer model construction, selection of retrieval spectra, and application of atmospheric parameter databases. Furthermore, this study provides an independently developed retrieval pathway for OMPS/LP, offering a complementary source for cross-validation with official products.

The study aims to demonstrate the effectiveness of the wavelength pairing and MART algorithm for retrieving OMPS/LP ozone profiles, thereby laying a theoretical and technical foundation for integrating OMPS/LP and OSIRIS data to construct long-term continuous datasets. The structure of this paper is as follows: Sect. 2 details the characteristics of the OMPS instrument, discussing its observational geometric principles and key issues in L1 data calibration. Section 3 systematically elaborates on the retrieval algorithm, including its core framework, application strategy of cloud filters, and parameter setting methods for the radiative transfer model. Section 4 conducts multi-dimensional validation and statistical analysis of the retrievals in this study, against NASA ozone profile products, MLS, OSIRIS, and ozonesonde datasets. Finally, the main results, key findings are summarized, and potential directions for future algorithm improvement are outlined in the conclusions.

## 2 OMPS/LP Ozone Retrieval

### 2.1 OMPS/LP instrument

The OMPS instrument was successfully launched aboard the SNPP satellite on 28 October 2011 (Zhu et al., 2025a). The satellite operates in a sun-synchronous polar orbit at an average altitude of 833 km with a 13:30 local time ascending node, commencing routine scientific observations in early 2012 (Kramarova et al., 2022). The OMPS suite integrates three distinct sensors: the Nadir Mapper (NM), Nadir Profiler (NP), and Limb Profiler (LP) (Flynn et al., 2014). Among them, OMPS/LP is centrally aimed at retrieving the vertical distribution of ozone in the Earth's middle atmosphere with high precision, employing a limb observation mode to sound the atmosphere by imaging the edge of the Earth's atmosphere. During a limb observation, the sensor's line-of-sight passes tangentially through the atmosphere, and the point along this path with the lowest altitude is termed the tangent point (TP). The vertical distance from this point to the Earth's geoid is referred to as the tangent height (TH). The

fundamental geometry of this observation mode is depicted in Fig. 1a.

The spectral coverage of OMPS/LP ranges from 290 to 1000 nm, with spectral resolution varying with wavelength from 1.5 nm at short wavelengths to 40 nm at the longer-wavelengths (Kramarova et al., 2014). Equipped with a charge-coupled device (CCD), the instrument can simultaneously observe scattered solar radiation across the full spectral range at altitudes from 0 to 100 km. Each detector pixel possesses an instantaneous vertical field of view of approximately 1.5 km. This configuration enables a high-precision vertical sampling of 1 km at the tangent point (Jaross et al., 2014). To expand cross-track coverage, OMPS/LP is configured with three observation slits horizontally spaced by 4.25° (approximately 250 km), whose observational geometry and field-of-view characteristics are illustrated in Fig. 1b. Each slit has a 1.85° vertical field of view (FOV), corresponding to a 110 km vertical observation range at the TP. This study focuses on measurement data from the central slit, which is aligned with the satellite's ground track. The SNPP satellite completes 14 orbits daily, with OMPS/LP performing approximately 160–180 measurements per orbit (at a latitudinal sampling interval of ~1°). LP can achieve global coverage every 3–4 d (Kramarova et al., 2024).

## 2.2 Key corrections in OMPS/LP L1G v2.6 data

Radiometric errors and sensor pointing errors are the two main error sources affecting limb-scattering ozone retrieval accuracy (Kramarova et al., 2024). The OMPS/LP L1G v2.6 dataset incorporates essential corrections to address these issues.

Pointing (altitude registration) corrections are applied to mitigate tangent height offsets caused by instrument alignment and thermal effects. Multi-point corrections include static, intra-orbit, and time-dependent adjustments following Moy et al. (2017).

Stray light correction is performed using an updated point spread function (PSF) based on pre-launch measurements (Jaross et al., 2014). In version 2.6, the PSF tail intensity in UV and VIS/NIR bands is increased by ~12% to improve high-altitude stray light estimation (Kramarova et al., 2024). An additional factor of 1.5 is applied in VIS/NIR wavelengths to correct for in-band scattering. While thermally induced wavelength shifts have negligible impact on height-normalized radiances in ozone retrieval, we note that residual wavelength-dependent errors could affect cross-section matching in regions of strong ozone absorption.

These calibration steps are critical for ensuring the radiometric and geometric accuracy of the radiances used in our retrieval. Further details can be found in the cited references.

## 3 Retrieval method

### 3.1 Retrieval vector

The retrieval method for vertical ozone concentration distributions based on OMPS/LP measurements in this study draws on the technical framework developed by Zhu et al. (2021), who derived ozone number density profiles using SCIAMACHY limb scattering measurements in the Chappuis–Wulf band. It shares similar methodological principles with the approaches proposed by Roth et al. (2007) and Degenstein et al. (2009), all of which employ retrieval vectors positively correlated with ozone concentrations for calculations.

The first step in the retrieval process involves normalizing the limb radiance at selected wavelengths. This operation entails normalizing the limb radiance at each wavelength to a reference TH, which effectively eliminates interference from the solar Fraunhofer structure, weakens the impact of surface reflection, and simultaneously achieves instrument self-calibration (Jia et al., 2015).

$$\mathbf{I}_{\text{nor}}(\lambda, \mathbf{H}) = \mathbf{I}(\lambda, \mathbf{H}) / \mathbf{I}(\lambda, H_{\text{ref}}) \quad (1)$$

where,  $\mathbf{H}$  denotes the TH, and  $\lambda$  represents the wavelength.  $\mathbf{I}(\lambda, H_{\text{ref}})$  and  $\mathbf{I}_{\text{nor}}(\lambda, \mathbf{H})$  refer to the radiance at the reference TH and the normalized radiance, respectively. The reference TH is an upper altitude where ozone sensitivity is low; in this study, it is selected as 40.5 km (i.e., the reference TH above the maximum retrieval altitude). Although radiance normalization cannot completely eliminate the influence of surface reflection or correct spectral errors such as wavelength shifts (which affect the calculation of ozone absorption cross-sections), it significantly reduces the requirements for both absolute radiometric calibration accuracy and modeling accuracy (Flittner et al., 2000). To mitigate the effect of aerosol scattering, the Chappuis triplet vector (CTV) method proposed by Degenstein et al. (2009) and Flittner et al. (2000) is employed for wavelength pairing. In the Chappuis–Wulf band, the CTV is defined as the difference between the logarithmic average of normalized radiances at two weakly ozone-absorbing wavelengths and the logarithm of the normalized radiance at a wavelength near the ozone absorption peak, thereby isolating the ozone absorption signal from common background scattering effects (e.g., aerosol scattering). It is expressed as:

$$\mathbf{y}_j = \ln \left( \frac{\sqrt{\mathbf{I}_{\text{nor}}(\lambda_{\text{ref1}}, j) \cdot \mathbf{I}_{\text{nor}}(\lambda_{\text{ref2}}, j)}}{\mathbf{I}_{\text{nor}}(\lambda_p, j)} \right) \quad (2)$$

where,  $j$  denotes the index of the TH measured by the instrument, and  $\mathbf{y}_j$  represents the retrieval vector after wavelength pairing at the  $j$ th of TH.  $\lambda_{\text{ref1}}$ ,  $\lambda_{\text{ref2}}$ , and  $\lambda_p$  correspond to the weakly ozone-absorbing reference wavelengths and the strongly absorbing peak wavelength, respectively.

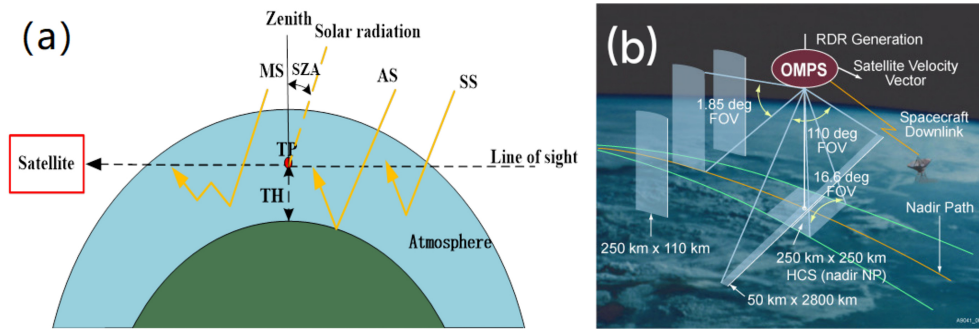


**Figure 1.** (a) Schematic of the satellite limb observation geometry, indicating the key parameters of tangent point (TP) and tangent height (TH) (SS: single scattering, AS: albedo scattering, MS: multiple scattering, SZA: solar zenith angle) (adapted from Arosio et al., 2018); (b) Schematic diagram of OMPS observation geometry and field-of-view characteristics (Kramarova et al., 2018).

In this study, the peak wavelength  $\lambda_p = 606.3$  nm corresponds to the visible channel configuration employed in the NASA OMPS/LP v2.6 operational algorithm (Kramarova et al., 2024), thereby ensuring consistency with established OMPS retrieval products. The weakly absorbing reference wavelengths  $\lambda_{\text{ref1}} = 512$  nm and  $\lambda_{\text{ref2}} = 675.5$  nm were optimized according to the selection criteria proposed by Zhu et al. (2021) for limb scattering ozone retrievals within the Chappuis-Wulf band, which take into account the specific spectral response and noise characteristics of OMPS/LP. Unlike the NASA algorithm, which uses spectral averages over multiple wavelengths for its visible triplet (510, 606, 675 nm; Kramarova and DeLand, 2023), the proposed method adopts individual discrete wavelength channels.

The CTV is designed to be positively correlated with ozone concentration (Degenstein et al., 2009). As expected, the CTV values and the retrieved ozone profiles show consistent vertical and latitudinal variations, with peak altitudes decreasing from the tropics to high latitudes. In this study, CTV values near zero above 35 km exhibit insufficient sensitivity to ozone, and values above 40 km become negative; therefore, the retrieval is restricted to altitudes below 40 km.

Aerosols, as suspended particles capable of absorbing and scattering light, have sources including both natural and anthropogenic factors. Stratospheric aerosols mainly originate from  $\text{SO}_2$ , HCl released by volcanic eruptions, naturally generated OCS, and pollutants such as  $\text{SO}_2$  from industrial emissions (Li et al., 2023b). The presence of aerosols enhances the intensity of atmospheric scattered light, with the effect being stronger at longer (red) wavelengths than at shorter (blue) wavelengths due to wavelength-dependent scattering. Based on the SCIATRAN model (radiative TRANSfer model for SCIAMACHY), this study conducted simulation experiments on aerosol extinction coefficients to explore their impacts on radiance and CTV.

Figure 2 shows the effects of aerosol extinction profiles perturbed with different scaling factors on radiance and CTV. We perturbed the aerosol extinction profiles with factors from 0.1 to 10 and we found that the radiance profile is

positively correlated with the aerosol extinction coefficient, while CTV decreases as the extinction coefficient increases, with the impact mainly concentrated below 30 km. For instance, when the aerosol extinction profile doubles, the radiance value at 21 km increases by 27 %, while CTV decreases by only 5 %. It indicates that wavelength pairing can weaken the aerosol scattering effect but cannot completely eliminate it. In addition, the study found that both radiance errors and CTV errors increase with an increase in SZA.

### 3.2 Multiplicative algebraic relaxation technology

Given the nonlinear nature of the retrieval problem, this study employs an iterative method for solution and selects the multiplicative algebraic reconstruction technique (MART) to perform ozone profile retrieval. As an improved algorithm of nonlinear relaxation techniques, MART has a main advantage in that it can utilize multiple sets of measurement vectors to realize the retrieval of atmospheric state parameters at any altitude (Roth et al., 2007). During the iteration process, the update of atmospheric states at each altitude depends on a multiplicative factor, which is obtained by weighted averaging the ratios of all valid observation vectors to simulation vectors. The general formula of the MART algorithm is as follows:

$$x_i^{(n+1)} = x_i^{(n)} \sum_j \left( \frac{y_j^{\text{obs}}}{y_j^{\text{mod}}} W_{ji} \right) = x_i^{(n)} \alpha_i \quad (3)$$

where,  $x_i^{(n)}$  denotes the ozone number density at atmospheric height  $i$  during the  $n$ th iteration;  $y_j^{\text{obs}}$  and  $y_j^{\text{mod}}$  represent the observation vector and simulation vector processed via Eqs. (1) and (2), respectively, where  $y^{\text{mod}}$  is generated by the radiative transfer model based on the ozone profile  $x^{(n)}$  obtained from the  $n$ th iteration;  $W_{ji}$  is the line-of-sight weight factor, indicating the importance of the  $j$ th TH or line of sight to the ozone retrieved at altitude  $i$ . At each altitude,  $\sum_j W_{ji} = 1$ . The value of  $W_{ji}$  in this study follows the setting

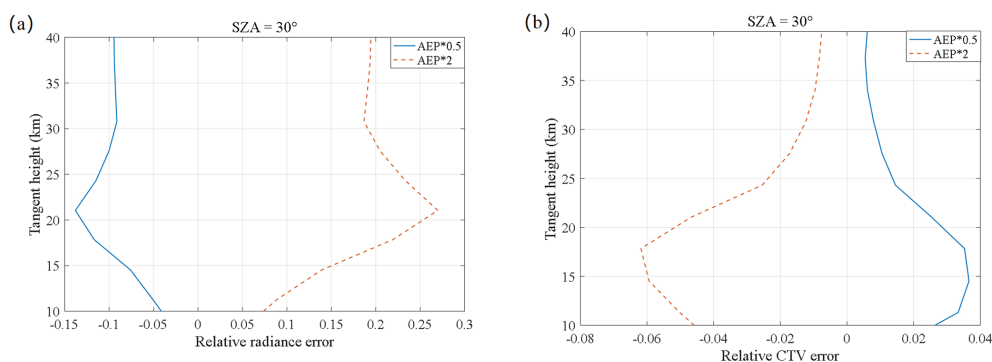


**Figure 2.** Variations in radiance and CTV due to perturbed aerosol extinction coefficients. (a) Relative radiance error; (b) Relative CTV error.

in Zhu et al. (2021).  $\alpha_i$  is the multiplicative update factors at atmospheric height  $i$ .

The sensitivity of retrieval to the true state and the contribution of prior information can be formally described through the averaging kernel and measurement response (Rodgers, 2000; von Clarmann et al., 2020). However, unlike Optimal Estimation (OE) approaches, the MART algorithm used in this study does not produce formal averaging kernels.

### 3.3 Cloud filter

A critical step in the OMPS/LP ozone profile retrieval is to define the lower boundary by determining the cloud top height. This is accomplished using a cloud detection method, modified from Chen et al. (2016), which leverages the spectral contrast in radiance between red and near-infrared bands. The method quantifies this contrast by computing the change in the vertical radiance gradient between two selected wavelengths. The underlying premise of the gradient-based cloud detection algorithm is that clouds generate a significantly larger radiance gradient compared to aerosols. This gradient is quantitatively defined as the rate of change of radiance with respect to TH:

$$G(\lambda, H) = \partial \ln I(\lambda, H) / \partial H \quad (4)$$

As shown in Fig. 3a, the variation characteristics of radiance gradient with wavelength in the 500–900 nm provide a basis for determining cloud top height. In cloud-free conditions, the radiance intensity varies slightly with wavelength; whereas in the presence of clouds, the wavelength dependence of radiance is significantly stronger than that of aerosols. Based on this, in this study, the cloud top height is determined by calculating the spectral gradient difference, with the formula as follows:

$$\ln R(H) = [G(\lambda_s, H) - G(\lambda_l, H)] \quad (5)$$

where,  $\lambda_s$  and  $\lambda_l$  denote the short wavelength and long wavelength, respectively. In this study,  $\lambda_s$  is set to 674 nm, and  $\lambda_l$  is set to 868 nm. The positive cloud detection threshold for

LP data is 1.5, which is also applicable to the detection of polar mesospheric clouds (PMCs). Taking the SNPP satellite orbit 51220 on 15 September 2021 as an example (Fig. 3b), the characteristics of  $\ln R$  profiles differ significantly between two cloudy events and one cloud-free event: the maximum value of  $\ln R$  in the cloud-free event is below 1.5, while that in the cloudy events is above this threshold, and the TH corresponding to the maximum  $\ln R$  value is the cloud top height. Retrievals are not performed below the cloud top height, while the multiplicative update factor above the cloud top is propagated downward into the cloudy region.

### 3.4 Implementation details

In this study, the SCIATRAN v2.2 toolbox (Rozanov et al., 2017) is employed as forward model to calculate the simulated radiances required for ozone concentration retrieval. The observed and simulated radiances are processed through normalization and wavelength pairing to form retrieval vectors, which serve as inputs to the MART algorithm to drive the iterative update of ozone profiles.

The radiative transfer solution in the forward model is based on the discrete ordinate method applied to a spherical atmosphere with a pseudo-spherical approximation for multiple scattering. The solution incorporates the effects of multiple scattering and refraction while explicitly omitting polarization. Radiance calculations in the model are focused solely on ozone, an absorbing gas, with the ozone absorption cross-sections taken from Bogumil et al. (2000). The pressure and temperature profiles used in this study were obtained from the Global Modeling and Assimilation Office (GMAO) interpolated dataset. These meteorological data are incorporated in the OMPS/LP L1G dataset provided by NASA (.2025a). In addition, the model sets the stratospheric background aerosol type as LOWTRAN (Kneizys, 1988), the boundary layer humidity as 80%, and the boundary layer aerosol type as marine. The retrieved ozone profiles are reported on the same vertical grid as the OMPS/LP L1G input data, which has a fixed spacing of 1 km in tangent height.

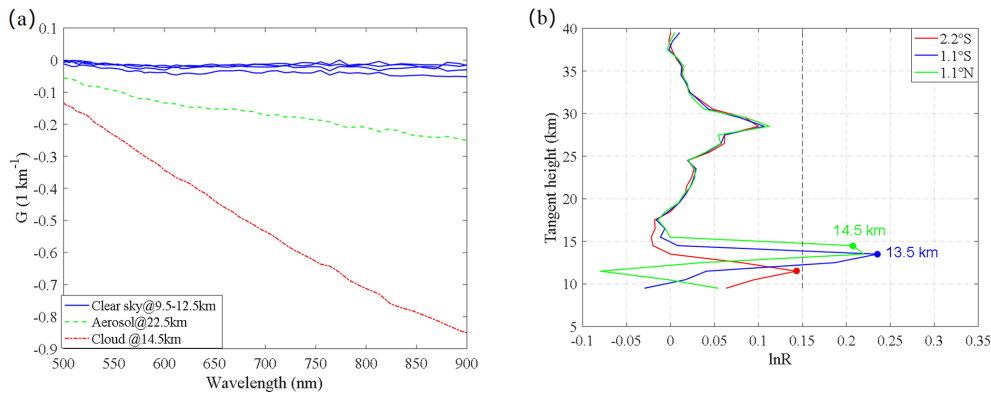


**Figure 3.** Radiance gradient  $G(\lambda, H)$  and gradient difference  $\ln R$  during orbit 51220 on 15 September 2021. **(a)** Radiance gradient  $G(\lambda, H)$  spectrum at  $3^\circ \text{N}$  under different atmospheric conditions: clear sky (blue), cloud (red), and aerosol (green); **(b)** Radiance gradient difference  $\ln R$  derived from OMPS/LP measurements for three equatorial events, showing the cloud detection results. The black dashed line represents the threshold employed for cloud identification.

However, this sampling interval does not imply an equivalent effective vertical resolution. The true vertical resolution is generally coarser than 1 km, particularly in regions of lower measurement sensitivity. The prior profiles are from SCIA-TRAN's built-in database. These profiles are provided by McLinden climatology (User's Guide for the software package SCIA-TRAN, 2018) and include monthly and latitude-dependent vertical distributions of volume mixing ratios for  $\text{O}_3$ ,  $\text{NO}_2$ ,  $\text{BrO}$ , and  $\text{OCIO}$ , as well as pressure and temperature in the 0 to 100 km altitude range.

## 4 Results

This section presents the processing results derived from the full year of 2021 OMPS-LP data. We utilized the L1G v2.6 dataset (Jaross, 2023), which incorporates enhanced stray light correction and pointing accuracy as detailed in Sect. 2.2. The analysis is based exclusively on measurements from the instrument's central slit.

### 4.1 Error analysis

In the field of error analysis on limb-scattering ozone retrieval, there is a wealth of academic studies. Zhu et al. (2022) used numerical perturbation to conduct formal error analysis on the retrieval method of the weighted multiplicative algebraic reconstruction technique, accurately quantifying ozone retrieval errors at different altitudes. Arosio et al. (2022) systematically evaluated random errors and systematic errors for stratospheric ozone profile retrieval based on OE algorithms. These research results provide important references for the error analysis of MART retrieval algorithm, and the error estimation results of this study are consistent with those in Arosio et al. (2022) and Zhu et al. (2022).

To ensure data quality, radiance measurements contaminated by clouds were systematically excluded during re-

trieval. Furthermore, the effective surface albedo was determined directly from OMPS/LP radiance measurements at 675 nm (referred to as scene reflectance in the NASA product), and the corrected THs provided in the NASA L1G data were adopted. Accordingly, the retrieval error budget focuses on four primary sources: prior profiles, aerosols extinction profile, ozone absorption cross-sections, and measurement noise.

We assess the sensitivity of the retrieval to the prior profile through a perturbation-based approach. In this study, the prior sensitivity analysis matrix  $\mathbf{A}_0$  is used to quantify the sensitivity of retrieval to the prior profile, and its expression is as follows:

$$\mathbf{A}_0 = \frac{\partial \hat{x}}{\partial \mathbf{x}_0} \quad (6)$$

where  $\mathbf{x}_0$  and  $\hat{x}$  represent the initial ozone profile and the retrieved ozone profile, respectively. To calculate the column vectors of  $\mathbf{A}_0$ , the ozone concentration at a single altitude was perturbed in  $\mathbf{x}_0$  by 5% and analyzes the corresponding changes in  $\hat{x}$ . Specifically,  $\partial \mathbf{x}_0$  is the perturbation applied to the prior, and  $\partial \hat{x}$  is the difference between the retrieval using the perturbed prior and the retrieval using the unperturbed prior.  $\mathbf{A}_0$  is a dimensionless matrix, whose characteristics can intuitively reflect the impact of changes in the prior profile on the retrievals.

Figure 4a illustrates the distribution of the prior sensitivity analysis matrix ( $\mathbf{A}_0$ ) column vectors across the 12–40 km altitude range, with each curve plotted at a vertical grid resolution of 1 km. A peak centered near the perturbation altitude indicates that the retrieval at that altitude retains sensitivity to the prior value at the same level. The width of the peak reflects the degree of vertical smoothing inherent in the retrieval. In the lower stratosphere (below 20 km), the response amplitudes are strong, indicating that strong prior dependence due to reduced measurement information con-

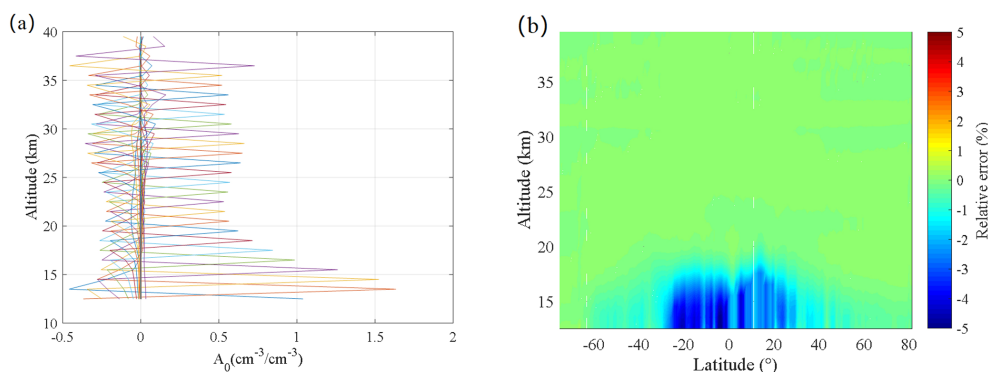


**Figure 4.** Examples of  $A_0$  (plotted every 1 km) and theoretical accuracy of prior profiles. (a) Distribution of  $A_0$  for measurements at 2.2° S; (b) Relative retrieval error resulting from a uniform +5 % perturbation of the entire prior profile (orbit 51220 on 15 September 2021).

tent under weak limb-scattering signals. This is consistent with the reduced information content of limb measurements in the upper troposphere and lower stratosphere, where the retrieval is primarily constrained by the prior.

While Fig. 4a illustrates the pattern of prior influence, it does not quantify the actual retrieval error that would result from an inaccurate prior. To assess this, the entire prior profile was uniformly scaled by +5 % at all altitudes, and the relative difference between the perturbed retrieval and the standard retrieval was computed. Figure 4b shows the relative error induced by a +5 % perturbation of the prior profile. Below 20 km, the retrieval shows sensitivity to the a priori, with relative errors  $-5\%$  in tropical regions. This indicates that a small increase in the prior profile leads to a noticeable underestimation of retrieved ozone concentrations in the tropical lower stratosphere, reflecting the high sensitivity of the retrieval to prior information in this region where measurement information content is low. With increasing altitude, the magnitude of the error progressively decreases. Above 25 km, the error approaches 0 % across all latitudes. At high latitudes, the error magnitude remains relatively small at all altitudes, indicating weaker prior dependence compared to tropical and mid-latitude regions.

The uncertainty of stratospheric aerosol extinction coefficients must be considered in the error budget for ozone profile retrievals. Previous studies have shown that retrieved aerosol extinction profiles have an average upper error bound of approximately 30 % in the lower stratosphere (Arosio et al., 2022). To assess the impact of this uncertainty on our ozone retrieval, we perturbed the climatological aerosol extinction profile by uniformly scaling it by +30 % at all altitudes and repeated the retrieval. The relative difference between the perturbed retrieval and the standard retrieval was then computed. Figure 5a depicts the resulting ozone retrieval errors as a function of latitude and altitude. It is evident that retrieval errors induced by variations in aerosol extinction coefficients are predominantly distributed within the 15–25 km altitude range, with a magnitude of approximately

5 %, and errors in the southern high latitudes are more pronounced. Within the 25–30 km range, the error is around 2 %, while above 30 km, it is less than 1 %. Below 15 km, errors vary with latitude, mostly falling within the range of  $\pm 2\%$ .

The temperature dependence of ozone absorption cross-sections has the potential to introduce errors in the retrieved profiles. To assess this effect quantitatively, we followed the approach which applied a uniform +2 % perturbations to the ozone absorption cross-sections at all temperatures used in the forward model. This perturbation magnitude represents a typical conservative estimate of cross-section uncertainty in the Chappuis band (Arosio et al., 2022). The retrieval was then repeated using the perturbed cross-sections, and the relative difference with respect to the standard retrieval was computed.

As shown in Fig. 5b, the resulting retrieval error exhibits a distinct vertical and latitudinal structure. In the tropics, the largest negative deviations ( $-3\%$  to  $-5\%$ ) appear below 20 km, indicating that retrievals in the tropical lower stratosphere are most sensitive to uncertainties in ozone absorption cross-sections. In the Southern Hemisphere (SH) mid-to-high latitudes, prominent negative deviations ( $-3\%$  to  $-4\%$ ) are found below 26 km. In the Arctic region, the negative bias below 20 km is relatively smaller, at approximately  $-2\%$ . Across all latitudinal bands, the error stabilizes near  $-2\%$  above 25 km. These results confirm that uncertainties in ozone absorption cross-sections introduce systematic biases in lower stratospheric ozone retrievals, especially in the tropics and SH mid-to-high latitudes. Specifically, a positive perturbation in the cross-sections leads to an underestimation of ozone concentrations, as observed in the negative biases in Fig. 5b.

To quantify the impact of random measurement noise on retrieval precision, a Monte Carlo simulation was performed using data from OMPS/LP orbit 51220. Sixteen representative latitudes spanning from 80° S to 80° N were selected. For each latitude, Gaussian random noise with a standard deviation of 1 % was added independently at each tangent height

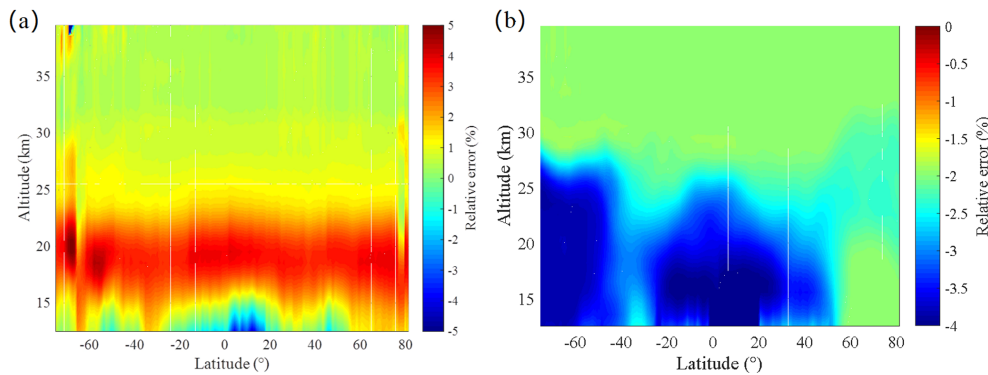


**Figure 5.** Distribution of relative errors in ozone retrieval with latitude and altitude, resulting from: (a) a +30 % uniform perturbation of the aerosol extinction profile; (b) a +2 % uniform perturbation of ozone absorption cross-sections at all temperatures.

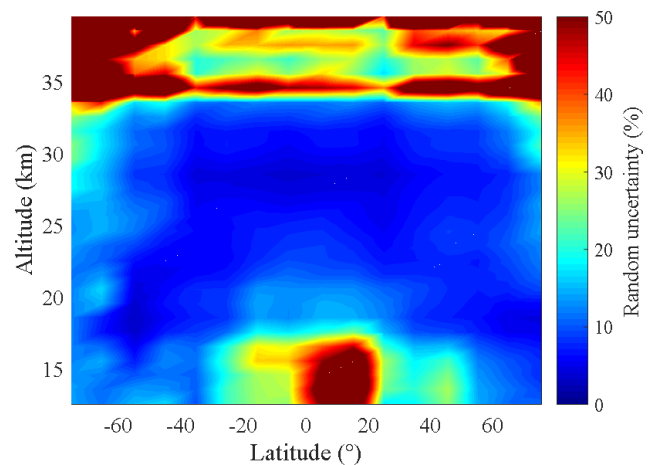
to the retrieval vector  $y_j$  (Eq. 2). This process was repeated 100 times, generating 100 independent noisy realizations per latitude. A full MART retrieval was conducted for each realization, producing an ensemble of 100 retrieved ozone profiles for each latitude. The random uncertainty due to measurement noise was quantified as the standard deviation of the 100 retrieved profiles at each altitude, expressed as a percentage of the average of the unperturbed profiles.

Figure 6 shows the latitudinal and altitudinal distribution of the resulting random uncertainty. Uncertainty remains low (< 10 %) at most latitudes within the 20–33 km mid-stratosphere, reflecting robust and stable retrieval performance. Above 30 km, especially at high latitudes, uncertainty increases sharply to above 20 %, which is mainly attributed to weaker signals in the visible spectral range. In the tropics below 20 km, a region of elevated uncertainty (> 15 %) is identified, likely associated with low ozone abundances, strong atmospheric variability, or reduced information content from the measurements.

## 4.2 Comparison with NASA OMPS-LP ozone product

The OMPS/LP v2.6 ozone profile retrieval algorithm developed by the NASA team is built on wavelength pairing and an optimal estimation with prior constraints (Kramarova and DeLand, 2023). This algorithm operates on combined UV-Vis measurement data from 12.5 km (or cloud top) to 57.5 km, producing a single ozone profile from each retrieval. The measurement vectors are obtained via doublet and triplet methods, with specific parameters detailed in Table 1. During algorithm implementation, the retrieved surface albedo, cloud top height, and corrected tangent height are incorporated. In the forward model, aerosol extinction coefficients retrieved from OMPS/LP measured data are used. For validation, only altitudes above the detected cloud top height are included in the comparison.

Figure 7 shows a comparison between the retrievals of this study and those of OMPS/LP v2.6, involving approximately 770 000 profiles. Among them, Fig. 7a presents an example



**Figure 6.** Random uncertainty in retrieved ozone profiles due to measurement noise, quantified as the standard deviation of 100 Monte Carlo realizations with 1 % Gaussian noise added to the retrieval vector.

**Table 1.** Parameters used in the OMPS/LP v2.6 ozone algorithm, according to Kramarova and DeLand (2023).

Parameters	Values
Wavelength used in UV (nm)	295, 302, 306, 312, 317, 322, 353
Wavelength used in Vis (nm)	510, 606, 675
Normalization Altitude in UV (km)	60.5 km
Normalization Altitude in Vis (km)	40.5 km

of number density for the annual average profile, and Fig. 7b shows the relative differences of the annual data. In this study, the relative difference is calculated as follows:

$$E_{\text{dif}} = \frac{2 \cdot ([\text{O}_3]_{\text{Ret}} - [\text{O}_3]_{\text{Ref}})}{([\text{O}_3]_{\text{Ret}} + [\text{O}_3]_{\text{Ref}})} \times 100 \% \quad (7)$$

where  $[O_3]_{Ret}$  denotes the ozone profile retrieved in this study, and  $[O_3]_{Ref}$  represents the reference ozone profile product.

As presented in Fig. 7b, the ozone concentrations from our retrieval systematically exceed those of the OMPS/LP v2.6 product at altitudes below 19 km and above 35 km. The positive deviation increases with decreasing altitude, reaching a maximum of approximately 10%–24% at the upper and lower retrieval boundaries. The ozone concentration is slightly lower between 20 and 28 km, with a deviation within 3%. There is an inherent negative deviation of about –6% around ~33 km. Overall, the deviation between 17 and 36 km is confined within 5%.

Figure 8 shows the mean relative differences between the retrievals of this study and OMPS/LP v2.6 in tropical regions and southern, northern mid-high latitudes. In the tropical regions within the 18–36 km altitude range, the deviation is within 5%, showing good consistency. At northern mid-high latitudes, the difference between 12 and 32 km reaches 8%, and the difference above 32 km is as high as 8%–13%, with similar deviations in the Arctic region. In the southern mid-high latitudes, most of the deviations above 18 km are less than 3%, but there is a positive deviation of up to 19% near 15 km. In the Antarctic region, this positive deviation reaches approximately 10% around 18 km.

The two datasets differ significantly in the upper troposphere and lower stratosphere (UTLS) region, especially in the tropical region, mainly due to the extremely low ozone concentration at this altitude. The large positive deviation at the upper boundary of retrieval is caused by the decreased ability of the visible spectrum to retrieve ozone at high altitudes, while the NASA product uses combined ultraviolet and visible spectrum information for retrieval at this altitude. Although there are differences between the retrievals of this study and the OMPS/LP v2.6 product in terms of ozone absorption cross-sections, prior profiles, aerosol settings, retrieval algorithms, and spectra, the overall consistency is high.

### 4.3 Comparison with MLS

The Earth Observing System-Microwave Limb Sounder (EOS-MLS) aboard the Aura satellite was successfully launched on 15 July 2004 (Waters et al., 2006). The satellite completes about 14 orbits daily, achieving global coverage between 82° S and 82° N. MLS provides vertical ozone profiles from the upper troposphere to the middle atmosphere using the 240 GHz frequency band by detecting naturally emitted microwave thermal radiation from the Earth's atmospheric limb measurements. Detailed descriptions can be found by Waters et al. (2006).

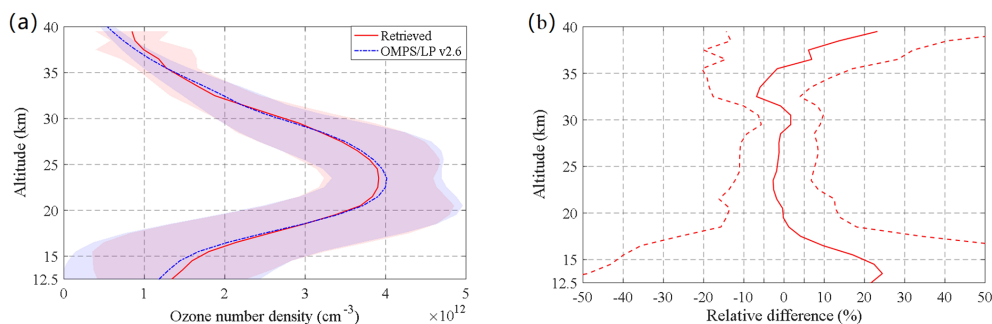
For validation purposes, this study employs the latest MLS L2 version 5.0 data product (Schwartz et al., 2020), with data filtering applied in accordance with the protocols recommended by Livesey et al. (2022). To ensure collocation

quality from the dataset, stringent criteria were enforced: we retained only those data pairs where the geographical separation between the OMPS/LP and MLS footprints was within 1° in both latitude and longitude, and the observation time difference was less than 6 h. In cases where multiple MLS profiles corresponded to a single OMPS/LP measurement, their average was computed and used. For consistent comparison with NASA products and ozonesonde data, the MLS volume mixing ratio (VMR) and pressure were first transformed to number density and altitude, utilizing the MLS geopotential height and temperature. These converted profiles were subsequently interpolated onto the regular altitude grid of the OMPS retrievals using a spline method.

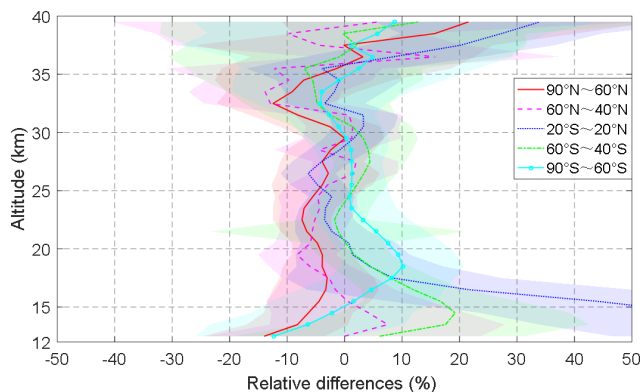
Figure 9 presents the average profiles and relative differences between the retrieval results of this study and MLS v5.0, involving approximately 93 000 profiles. The results show that compared with MLS v5.0, the ozone concentration retrieved in this study has a relatively large positive deviation of 5%–20% below 18 km; the positive deviation above 32 km increases with altitude; within the 18–35 km height range, the deviation between the two is confined within 5%.

Figure 10 shows the mean relative differences in five latitude zones, with shaded areas indicating the standard deviations. In terms of data sample size, there are approximately 18 000 profiles in the tropical region, about 20 000 in the northern high latitudes, and around 15 000 in the southern high latitudes. The analysis results reveal that within the 12–35 km height range, the zonal average relative differences in each latitude zone are basically confined within 10%. Among them, the northern mid-high latitudes exhibit a stable negative deviation of 5%–10% at 20–35 km; the southern mid-latitudes have a constant positive deviation of 1%–5% at 18–36 km, which increases to 3%–10% in the polar regions. In the tropical regions the differences change sign with altitude: the retrieved ozone number density at 19–27 km is 5%–10% lower than that of MLS, while it is 3%–10% higher in the 28–36 km range. It is worth noting that below 19 km, the consistency between the retrieval results of this study and MLS data decreases significantly, with the relative difference in the tropical region even exceeding 30%, although the absolute difference is relatively small (see Fig. 10a).

Figure 11 depicts the altitude-dependent relative differences between retrieved profiles and MLS zonal means in 1° latitude bins across the three selected periods. The full-year 2021 data shown in Fig. 11a indicate that within the 20–35 km altitude range, differences across all latitudes are basically confined within  $\pm 10\%$ . The altitude-dependent behavior of the retrieval biases can be summarized as follows. In the tropical UTLS region, oscillating differences exceeding 30% are observed, which may be attributed to several factors: the highly dynamic variability of ozone concentrations, the limited detection sensitivity at the lowest retrieval altitudes, and the influence of cloud filtering. Furthermore, the inherently low ozone abundance in this region exacer-



**Figure 7.** (a) Annual mean ozone number density profiles from this study and OMPS/LP v2.6, with shaded areas indicating the standard deviation. (b) The corresponding annual mean relative differences calculated pairwise for each collocated measurement using Eq. (7), with the standard deviation shown as a dashed line.



**Figure 8.** Zonal mean relative differences (this study vs. OMPS/LP v2.6) across five latitudinal bands (60–90° N, 40–60° N, 20° S–20° N, 60–40° S, 90–60° S); standard deviations are shown as shaded areas.

bates the discrepancies in relative values. A distinct negative bias in retrieved ozone values is evident at 20–23 km in the tropics, particularly pronounced during winter (Fig. 11c). Conversely, a positive bias is observed over Antarctica, possibly linked to inaccuracies in the retrieved effective surface albedo, particularly in polar regions with high seasonal variability. Above 35 km, the retrievals exhibit a positive bias in the tropics. This bias arises from the inherently limited sensitivity of the visible spectrum at these altitudes, where ozone absorption is weak and measurement signals become dominated by noise and stray light.

In summary, the comparative analysis of this study shows that the effectiveness of OMPS retrieval varies across different regions and altitudes: the accuracy in tropical regions is concentrated in the 20–35 km altitude range; in mid-latitude regions, good consistency is also observed below 15 km. Nevertheless, in some atmospheric regions and under different seasonal conditions, the relative deviation may still exceed 10 % compared with MLS data.

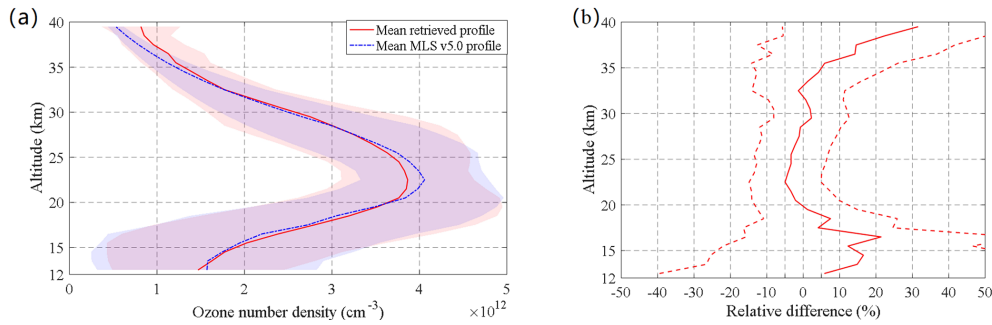
#### 4.4 Comparison with OSIRIS

In February 2001, the OSIRIS instrument was launched aboard the Odin satellite into a nearly circular sun-synchronous orbit (Llewellyn et al., 2004). The orbit has an altitude of approximately 600 km, an orbital period of 96 min, an inclination of 97.8°, and covers an observational latitude range from 82° S to 82° N. The satellite's ascending node crosses the equator at approximately 18:00 local time. Detailed descriptions of the instrument can be found by Llewellyn et al. (2004). Degenstein et al. (2009) used the MART to retrieve ozone profiles in the altitude range from 10 km or cloud top to 60 km, with the retrieval algorithm integrating radiation information from the UV and VIS bands. In this study, the version of OSIRIS L2 v7.3 data (University of Saskatchewan, 2025) is used for verification.

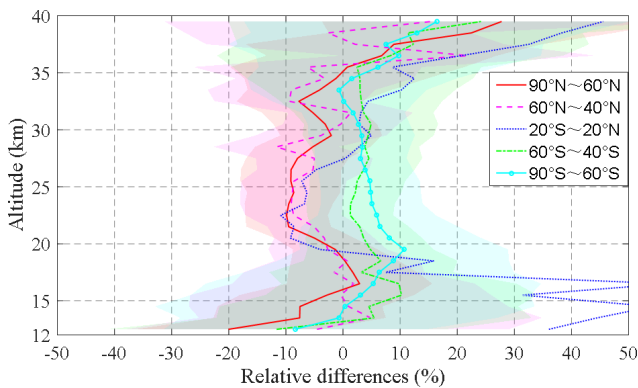
Owing to the sparsity of coincident OSIRIS measurements, a relaxed collocation criterion was adopted. Data pairs were considered matched if the geographical distance between the instrument footprints was within 2° in latitude and 5° in longitude, and the time difference was within 24 h. When multiple OMPS/LP profiles corresponded to a single OSIRIS observation, their average was used. To unify the data format, the ozone concentration unit ( $\text{mol m}^{-3}$ ) of OSIRIS profiles is converted to number density ( $\text{molecule cm}^{-3}$ ).

Figure 12 shows the average profiles and relative differences between the retrieval results of this study and OSIRIS v7.3, involving approximately 44 000 profiles. The results indicate that compared with OSIRIS v7.3, the ozone concentration retrieved in this study has a relatively large positive deviation of 28 %–34 % below 18 km; above 35 km, the positive deviation increases with increasing altitude; in the 20–35 km altitude range, except near 23 km, most of the deviations between the two are confined within 5 %.

Figure 13 further compares the mean relative differences of the five latitude zones, with shaded areas indicating the standard deviations. In terms of data sample size, there are approximately 17 000 profiles in the tropical region, about



**Figure 9.** (a) Annual mean ozone number density profiles from this study and MLS v5.0, accompanied by standard deviations (shaded areas). (b) The corresponding annual mean relative differences calculated pairwise for each collocated measurement using Eq. (7), with the standard deviation shown as a dashed line.



**Figure 10.** Zonal mean relative differences for (this study vs. MLS v5.0) five latitudinal bands (60–90° N, 40–60° N, 20° S–20° N, 60–40° S, 90–60° S); standard deviations as shaded areas.

10 000 in the northern high latitudes, and around 7000 in the southern high latitudes. The analysis shows that the northern mid-high latitudes have a significant negative deviation of 5 %–13 % at 21–25 km altitude, which is more prominent in polar regions; the difference in the southern mid-latitudes at 20–36 km altitude is less than 4 %, and the consistency in the Antarctic region at 23–35 km altitude is better than 2.5 %; most of the deviations in the tropical region at 26–36 km altitude are within 2 %. In addition, the differences in the region below 20 km are significant, with the relative difference in the tropical region exceeding 50 % and reaching 30 % at 13 km in the southern mid-latitude zone.

#### 4.5 Comparison with ozonesondes

To robustly validate the retrieved ozone concentrations at altitudes below 30 km, this study employs a comparative analysis with ozonesonde measurements. The sonde data were obtained from the World Ozone and Ultraviolet Radiation Data Centre (WOUDC) and the Southern Hemisphere Additional Ozonesondes (SHADOZ) network (Thompson et al., 2007). Accounting for the sparse spatial distribution of ozonesonde

stations, a relaxed collocation criterion was implemented: an OMPS/LP measurement was considered a match if it fell within  $\pm 5^\circ$  latitude and  $\pm 10^\circ$  longitude of a sonde station and occurred within  $\pm 12$  h of its launch. For each ozonesonde profile, all collocated OMPS/LP retrievals were averaged to form a single comparative data point.

In quantitative comparisons, to align the vertical resolution of ozonesonde data with that of OMPS data, a moving average filtering method is used for dimensionality reduction of ozonesonde data. The specific procedure begins with defining the window size of the moving average filter:

$$N = \frac{\Delta z_{\text{low}}}{\Delta z_{\text{high}}} \quad (8)$$

where,  $\Delta z_{\text{low}}$  and  $\Delta z_{\text{high}}$  represent the low vertical resolution of OMPS data and the high vertical resolution of ozonesonde data, respectively.

Filtering is applied to the original ozonesonde data  $x_{\text{fine}}$  to obtain the dimensionality-reduced data  $x_{\text{coarse}}$ , which is expressed as:

$$x_{\text{coarse}}(z_k) = \frac{1}{2N + 1} \sum_{j=-N}^N x_{\text{fine}}(z_{k+j}) \quad (9)$$

where  $z_k$  denotes the altitude, and  $k$  represents the layer index.

In addition, another processing approach involves convolving ozonesonde measurements with the averaging kernels (AKs) retrieved from OMPS/LP v2.6 (see Arosio et al., 2018 for details). Taking the Alert station (82.5° N, 62.4° W) as an example, Fig. 14 presents the comparison results between the ozonesonde data and the collocated OMPS average profile on 15 September 2021. It is found that there are differences in the dimensionality-reduced ozonesonde data obtained by the two methods. The data curve processed by convolution with averaging kernels is smoother and its shape is closer to the OMPS product; while the data processed by moving average filter retains more original features with a sharper curve. After comprehensive consideration, the mov-

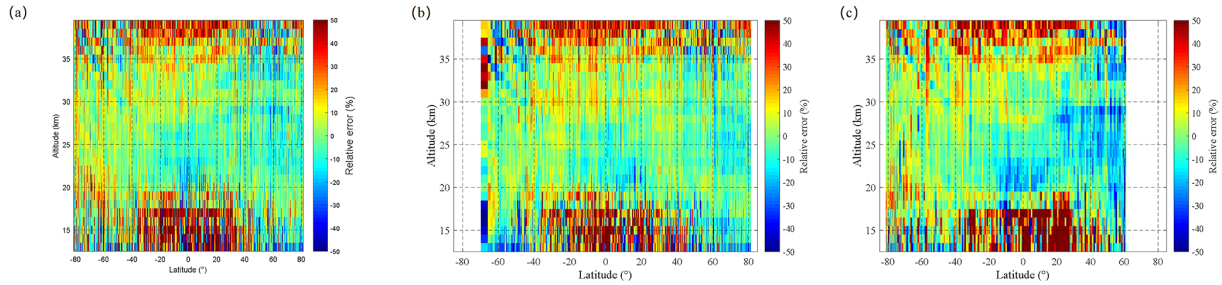


**Figure 11.** Relative differences in ozone number density, averaged over 1° latitude bins and plotted as a function of altitude, for (a) the entire year of 2021, (b) the boreal summer months (June–August), and (c) December.

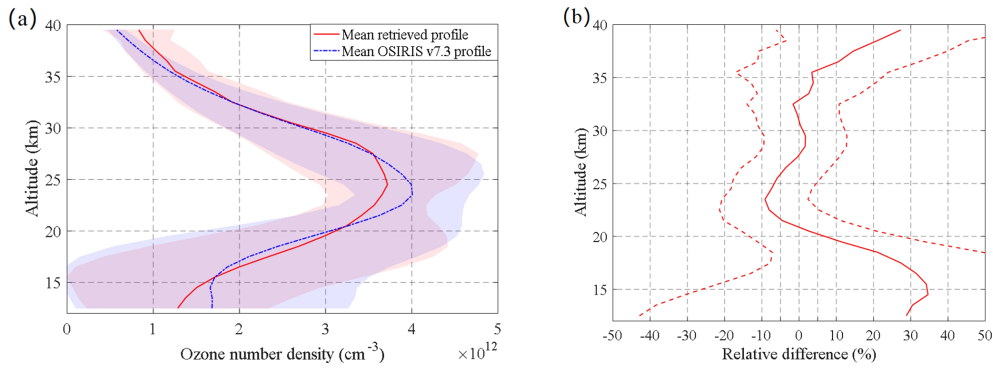


**Figure 12.** (a) Annual mean ozone number density profiles from this study and OSIRIS v7.3, accompanied by standard deviations (shaded areas); (b) The corresponding annual mean relative differences calculated pairwise for each collocated measurement using Eq. (7), accompanied by standard deviations (dashed lines).

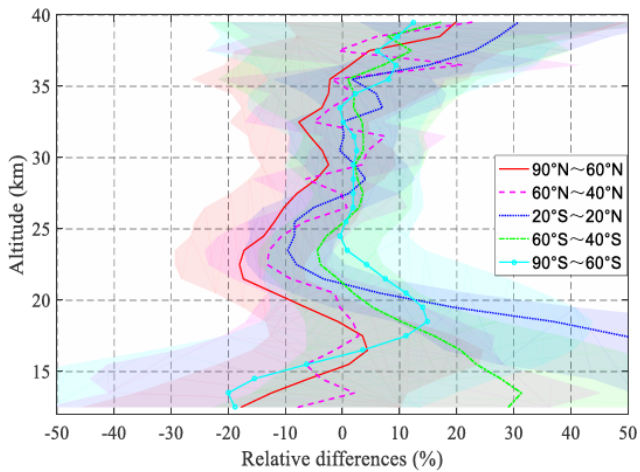


**Figure 13.** Zonal mean relative differences (this study vs. OSIRIS v7.3) for five latitudinal bands (60–90° N, 40–60° N, 20° S–20° N, 60–40° S, 90–60° S); standard deviations as shaded areas.

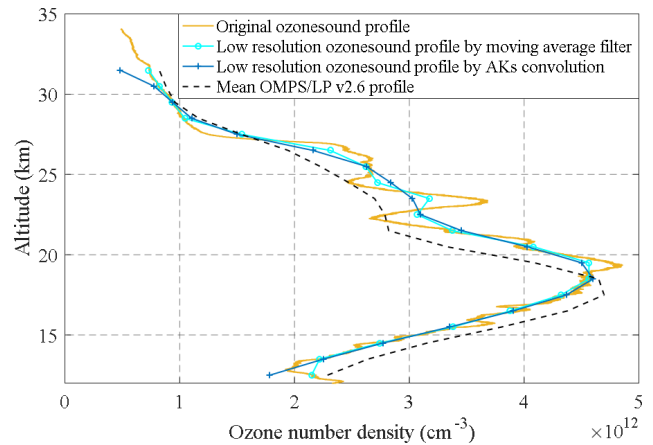
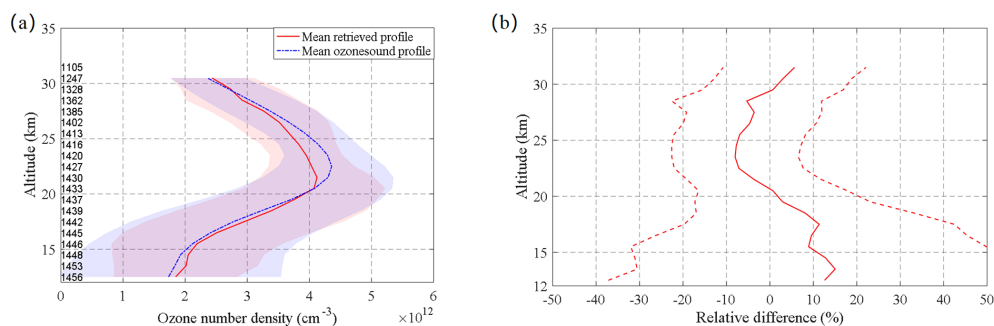


**Figure 14.** Ozonesonde data and OMPS collocated average profiles at Alert station on 15 September 2021.

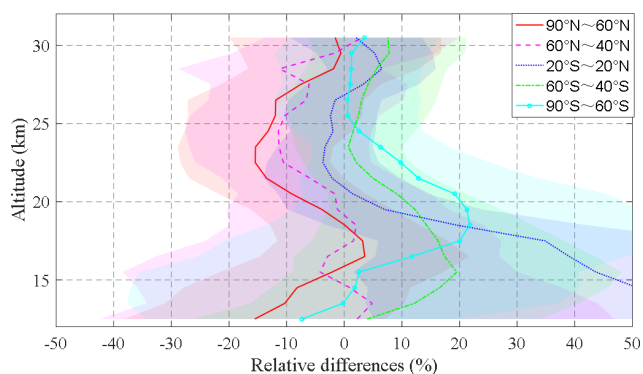
ing average filter is finally adopted for data processing in this study.

Figure 15 presents the annual average collocated profiles and their relative differences. The left side of the figure indicates the number of valid collocations at each altitude,

with the total sample size amounting to approximately 1460. This study included data from 41 ozonesonde stations, involving over 1700 individual profiles. A significant positive bias of 10%–15% is observed in the retrievals compared to ozonesonde data below 18 km, while the deviation generally stays within 10% across the 15–30 km altitude range.



**Figure 15.** (a) Annual mean collocated ozone number density profiles from this study and ozonesonde measurements, accompanied by standard deviations (shaded areas). (b) Mean relative differences calculated pairwise for each collocated measurement using Eq. (7), accompanied by standard deviations (dashed lines).



**Figure 16.** Zonal mean relative differences (this study vs. ozonesondes) for five latitudinal bands (60–90° N, 40–60° N, 20° S–20° N, 60–40° S, 90–60° S); standard deviations as shaded areas.

Figure 16 presents the mean relative differences across five latitude zones. The number of available collocations in the tropical and Antarctic regions is approximately 200 and 75, respectively. Specifically, the tropical region shows good consistency above 20 km, with most relative differences within  $\pm 4\%$  between 20 and 30 km. The southern mid-latitude region also exhibits high consistency, with positive biases generally less than 5% above 20 km, but a relatively large positive bias of about 19% near 15 km. In the Antarctic region, the bias is less than 2% above 25 km, while significant differences occur below 25 km, with a positive bias as high as 21% at 19 km. The northern mid-latitude zone has a bias of less than 5% below 21 km, but a constant negative bias of 5%–11% between 21–28 km, and this negative bias is more pronounced in the Arctic region.

## 5 Conclusions

This study innovatively applies an ozone profile retrieval method – originally developed at the University of Saskatchewan for OSIRIS measurements and based on wavelength pairing and the MART – to OMPS/LP observations.

After processing and analyzing the 2021 annual OMPS/LP v2.6 L1G data, observations with the instrument's central slit and solar zenith angle less than  $85^\circ$  were selected, and ozone profiles between 12.5 and 39.5 km were retrieved. A comprehensive multi-dimensional validation was conducted.

Comparison with the NASA L2 v2.6 official product shows that the overall consistency is good across latitude zones at 20–36 km, with most differences within  $\pm 5\%$ . However, differences near 33 km in the northern mid-latitudes and polar regions reach up to 10%. Below 20 km, ozone concentrations are relatively high in the Antarctic ozone peak region, with a pronounced positive bias around 15 km in tropical and southern mid-latitude zones.

Validation against MLS v5.0 and OSIRIS v7.3 ozone profiles, as well as ozonesonde data from SHADOZ and WOUDC, indicates that relative differences with MLS are mostly within  $\pm 10\%$  between 13 and 35 km, except for significant discrepancies in the tropical UTLS region. Compared to OSIRIS v7.3, a negative bias of 13%–18% occurs at 20–25 km in northern mid-high latitudes, while positive biases reach 18% at 18 km over Antarctica and exceed 20% at 15 km in southern mid-latitudes, with more pronounced deviations in the tropics. Relative to ozonesonde data, differences in tropical and southern mid-latitude regions at 20–30 km remain within  $\pm 4\%$ , whereas differences of 11%–15% are observed at 20–25 km in northern mid-high latitudes. Consistency is good below 20 km in northern mid-latitudes, but positive biases reach 21% at 18 km over Antarctica and 19% at 15 km in southern mid-latitudes.

Overall, compared with the reference products, the retrieved ozone concentrations in this study exhibit biases mostly within 5% between 25 and 35 km. A negative bias of 5%–10% is observed at 20–25 km in northern mid-high latitudes, particularly in the Arctic. Retrieved values are about 10% higher at the altitude of the Antarctic ozone concentration peak, 10%–15% higher at 15 km in southern mid-latitudes, and over 30% higher below 20 km in the tropics.

The identified biases mainly originate from three factors. Below 20 km, cloud effects remain non-negligible. A sen-

sitivity test on a representative profile (equatorial region) demonstrates that, at the same altitudes above the CTH, our method – which propagates the multiplicative update factor from above the cloud top into the cloudy region – produces ozone concentrations approximately 25 % higher than the scheme with retrieval limited only to altitudes above the cloud top. This result quantitatively reveals the potential systematic impact of cloud constraints on ozone profile retrievals under cloudy conditions. These discrepancies are further exacerbated by low ozone abundance, strong dynamical variability in the tropics, and the reduced sensitivity of limb retrievals at lower altitudes, while inconsistencies between the background aerosols used in retrievals and real atmospheric conditions also contribute. Beyond aerosol effects, additional bias contributions arise from ozone absorption cross-sections that incompletely account for temperature-dependent uncertainties, as well as the neglect of NO<sub>2</sub> absorption in the current forward model. The overestimation of ozone abundances above 35 km across all latitudes results from the limited sensitivity of the visible spectrum for high-altitude ozone retrievals, in contrast to the operational product that employs combined ultraviolet and visible spectral information.

Based on these findings, several priorities for follow-up research are identified. First, integrating operational aerosol extinction products from NASA will be essential to replace the current climatological approach and reduce systematic biases in the UTLS region. Further model improvements will include updating the ozone absorption cross-section database and incorporating NO<sub>2</sub> absorption into the forward model. Second, including ultraviolet channels will improve retrieval accuracy above 35 km, where visible-only measurements have low sensitivity. Third, refining cloud filtering will better constrain lower altitude retrievals. Finally, the consistent retrieval core shared with OSIRIS lays a solid technical foundation for constructing long-term, coherent stratospheric ozone records, thereby minimizing discrepancies in multi-satellite data merging and supporting climate studies that require stable, multi-decadal observational records.

**Data availability.** Ancillary information and v2.6 L1G OMP-S/LP data were downloaded from <https://disc.gsfc.nasa.gov/datasets> (NASA, 2025a), where L2 data are also available. For the validation sections, MLS L2 data were also taken from <https://doi.org/10.5067/Aura/MLS/DATA2516> (Schwartz et al., 2020). OSIRIS v7.3 data were taken from <https://research-groups.usask.ca/osiris/data-products.php> (University of Saskatchewan, 2025). WOUDC data were downloaded on 10 April 2025 from <https://woudc.org/data/explore.php> (last access: 10 April 2025). A list of all contributors is available on the following website: <https://woudc.org/contributors/> (last access: 10 April 2025). SHADOZ data were downloaded on 21 April 2025 from <https://tropo.gsfc.nasa.gov/shadoz/Archive.html> (NASA, 2025b).

**Author contributions.** FZ designed the retrieval algorithm to OMP-S/LP observations, processed the data set, performed the validation of the results and wrote the manuscript. FZ and SWL proposed the research and lead the project, analyzed the results and contributed to the writing of the manuscript and the scientific outcomes. XPL contributed the algorithm for cloud filtering, and reviewed the paper. FQS supervised and guided the retrieval process and reviewed the paper.

**Competing interests.** The contact author has declared that none of the authors has any competing interests.

**Disclaimer.** Publisher's note: Copernicus Publications remains neutral with regard to jurisdictional claims made in the text, published maps, institutional affiliations, or any other geographical representation in this paper. The authors bear the ultimate responsibility for providing appropriate place names. Views expressed in the text are those of the authors and do not necessarily reflect the views of the publisher.

**Acknowledgements.** This work was supported by the National Science Foundations of China (grant no. 41875040), and partially funded by the Excellent Research and Innovation Team of Anhui Provincial Department of Education (grant no. 2023AH010043)

We would like to express our sincere gratitude to the NASA OMPS SIPS team for providing data support. We are also thankful to the SCIATRAN radiative transfer model development team.

**Financial support.** This research has been supported by the National Science Foundations of China (grant no. 41875040), the Excellent Research and Innovation Team of Anhui Provincial Department of Education (2023AH010043).

**Review statement.** This paper was edited by Lars Hoffmann and reviewed by two anonymous referees.

## References

- Arosio, C., Rozanov, A., Malinina, E., Eichmann, K.-U., von Clar-mann, T., and Burrows, J. P.: Retrieval of ozone profiles from OMPS limb scattering observations, *Atmos. Meas. Tech.*, 11, 2135–2149, <https://doi.org/10.5194/amt-11-2135-2018>, 2018.
- Arosio, C., Rozanov, A., Gorschelev, V., Laeng, A., and Burrows, J. P.: Assessment of the error budget for stratospheric ozone profiles retrieved from OMPS limb scatter measurements, *Atmos. Meas. Tech.*, 15, 5949–5967, <https://doi.org/10.5194/amt-15-5949-2022>, 2022.
- Bernath, P. F., McElroy, C. T., Abrams, M. C., Boone, C. D., Butler, M., Camy-Peyret, C., Carleer, M., Clerbaux, C., Coheur, P. F., Colin, R., DeCola, P., De Mazière, M., Drummond, J. R., Dufour, D., Evans, W. F. J., Fast, H., Fussen, D., Gilbert, K., Jennings, D. E., Llewellyn, E. J., Lowe, R. P., Mahieu, E., Mc-

- Connell, J. C., McHugh, M., McLeod, S. D., Michaud, R., Midwinter, C., Nassar, R., Nichitiu, F., Nowlan, C., Rinsland, C. P., Rochon, Y. J., Rowlands, N., Semeniuk, K., Simon, P., Skelton, R., Sloan, J. J., Soucy, M.-A., Strong, K., Tremblay, P., Turnbull, D., Walker, K. A., Walkty, I., Wardle, D. A., Wehrle, V., Zander, R., and Zou, J.: Atmospheric Chemistry Experiment (ACE): Mission overview, *Geophys. Res. Lett.*, 32, L15S01, <https://doi.org/10.1029/2005GL022386>, 2005.
- Bertaux, J. L., Kyrölä, E., Fussen, D., Hauchecorne, A., Dalaudier, F., Sofieva, V., Tamminen, J., Vanhellefont, F., Fanton d'Andon, O., Barrot, G., Mangin, A., Blanot, L., Lebrun, J. C., Pérot, K., Fehr, T., Saavedra, L., Leppelmeier, G. W., and Fraisse, R.: Global ozone monitoring by occultation of stars: an overview of GOMOS measurements on ENVISAT, *Atmos. Chem. Phys.*, 10, 12091–12148, <https://doi.org/10.5194/acp-10-12091-2010>, 2010.
- Bogumil, K., Orphal, J., and Burrows, J. P.: Temperature dependent absorption cross sections of O<sub>3</sub>, NO<sub>2</sub>, and other atmospheric trace gases measured with the SCIAMACHY spectrometer, in: *Proceedings of the ERS-Envisat-Symposium*, Goteborg, Sweden, 2000.
- Burrows, J., Hölzle, E., Goede, A., Visser, H., and Fricke, W.: SCIAMACHY–Scanning imaging absorption spectrometer for atmospheric cartography, *Acta Astronaut.*, 35, 445–451, [https://doi.org/10.1016/0094-5765\(94\)00278-T](https://doi.org/10.1016/0094-5765(94)00278-T), 1995.
- Chen, Z., DeLand, M., and Bhartia, P. K.: A new algorithm for detecting cloud height using OMPS/LP measurements, *Atmos. Meas. Tech.*, 9, 1239–1246, <https://doi.org/10.5194/amt-9-1239-2016>, 2016.
- Chipperfield, M. P. and Bekki, S.: Opinion: Stratospheric ozone – depletion, recovery and new challenges, *Atmos. Chem. Phys.*, 24, 2783–2802, <https://doi.org/10.5194/acp-24-2783-2024>, 2024.
- Cisewski, M., Zawodny, J., Gasbarre, J., Eckman, R., Topiwala, N., Rodriguez-Alvarez, O., Cheek, D., and Hall S.: The Stratospheric Aerosol and Gas Experiment (SAGE III) on the International Space Station (ISS) Mission, in: *Proceedings 9241, Sensors, Systems, and Next-Generation Satellites XVIII, SPIE Remote Sensing*, Amsterdam, Netherlands, <https://doi.org/10.1117/12.2073131>, 2014.
- Degenstein, D. A., Bourassa, A. E., Roth, C. Z., and Llewellyn, E. J.: Limb scatter ozone retrieval from 10 to 60 km using a multiplicative algebraic reconstruction technique, *Atmos. Chem. Phys.*, 9, 6521–6529, <https://doi.org/10.5194/acp-9-6521-2009>, 2009.
- DeLand, M., Bhartia, P., Xu, P., Kramarova, N., and Zhu, T.: OMPS Limb Profiler Ozone Product O<sub>3</sub>: Version 2.5 Data Release Notes, [https://snpp-omps.gesdisc.eosdis.nasa.gov/data/SNPP\\_OMPS\\_Level2/OMPS\\_NPP\\_LP\\_L2\\_O3\\_DAILY.2/doc/README.OMPS\\_NPP\\_LP\\_L2\\_O3\\_DAILY.2.pdf](https://snpp-omps.gesdisc.eosdis.nasa.gov/data/SNPP_OMPS_Level2/OMPS_NPP_LP_L2_O3_DAILY.2/doc/README.OMPS_NPP_LP_L2_O3_DAILY.2.pdf) (last access: 4 September 2025), 2017.
- Flittner, D. E., Bhartia, P. K., and Herman, B. M.: O<sub>3</sub> Profiles Retrieved from Limb Scatter Measurements: Theory, *Geophys. Res. Lett.*, 27, 2601–2604, <https://doi.org/10.1029/1999GL011343>, 2000.
- Flynn, L., Long, C., Wu, X., Evans, R., Beck, C., Petropavlovskikh, I., McConville, G., Yu, W., Zhang, Z., Niu, J., Beach, E., Hao, Y., Pan, C., Sen, B., Novicki, M., Zhou, S., and Seftor, C.: Performance of the ozone mapping and profiler suite (OMPS) products, *J. Geophys. Res.-Atmos.*, 119, 6181–6195, <https://doi.org/10.1002/2013JD020467>, 2014.
- Jaross, G.: OMPS-NPP L1G LP Radiance EV Wavelength-Altitude Grid swath orbital 3slit V2.6, Greenbelt, MD, USA, Goddard Earth Sciences Data and Information Services Center (GES DISC), <https://doi.org/10.5067/YVE3FSNJ59RQ>, 2023.
- Jaross, G., Bhartia, P. K., Chen, G., Kowitz, M., Haken, M., Chen, Z., Xu, P., Warner, J., and Kelly, T.: OMPS Limb Profiler instrument performance assessment, *J. Geophys. Res.-Atmos.*, 119, 4399–4412, <https://doi.org/10.1002/2013JD020482>, 2014.
- Jia, J., Rozanov, A., Ladstätter-Weissenmayer, A., and Burrows, J. P.: Global validation of SCIAMACHY limb ozone data (versions 2.9 and 3.0, IUP Bremen) using ozonesonde measurements, *Atmos. Meas. Tech.*, 8, 3369–3383, <https://doi.org/10.5194/amt-8-3369-2015>, 2015.
- Kneizys, F. X.: Users Guide to LOWTRAN 7[M], Air Force Geophysics Laboratory, 1988.
- Kramarova, N. A.: OMPS-NPP L2 LP Ozone (O<sub>3</sub>) Vertical Profile swath daily Center slit V2.6, Greenbelt, MD, USA, Goddard Earth Sciences Data and Information Services Center (GES DISC), <https://doi.org/10.5067/8MO7DEDYTBH7>, 2023.
- Kramarova, N. A. and DeLand, M.: OMPS Limb Profiler Ozone Product O<sub>3</sub>: Version 2.6 Data Release Notes, 36 pp., [https://omps.gesdisc.eosdis.nasa.gov/data/SNPP\\_OMPS\\_Level2/OMPS\\_NPP\\_LP\\_L2\\_O3\\_DAILY.2.6/doc/README.OMPS\\_NPP\\_LP\\_L2\\_O3\\_DAILY\\_V2.6.pdf](https://omps.gesdisc.eosdis.nasa.gov/data/SNPP_OMPS_Level2/OMPS_NPP_LP_L2_O3_DAILY.2.6/doc/README.OMPS_NPP_LP_L2_O3_DAILY_V2.6.pdf) (last access: 5 March 2025), 2023.
- Kramarova, N. A., Nash, E. R., Newman, P. A., Bhartia, P. K., McPeters, R. D., Rault, D. F., Seftor, C. J., Xu, P. Q., and Labow, G. J.: Measuring the Antarctic ozone hole with the new Ozone Mapping and Profiler Suite (OMPS), *Atmos. Chem. Phys.*, 14, 2353–2361, <https://doi.org/10.5194/acp-14-2353-2014>, 2014.
- Kramarova, N. A., Bhartia, P. K., Jaross, G., Moy, L., Xu, P., Chen, Z., DeLand, M., Froidevaux, L., Livesey, N., Degenstein, D., Bourassa, A., Walker, K. A., and Sheese, P.: Validation of ozone profile retrievals derived from the OMPS LP version 2.5 algorithm against correlative satellite measurements, *Atmos. Meas. Tech.*, 11, 2837–2861, <https://doi.org/10.5194/amt-11-2837-2018>, 2018.
- Kramarova, N. A., Xu, P., Mok, J., Bhartia, P. K., Jaross, G., Moy, L., Weaver, C., Frith, S., Ziemke, J., Chen, Z., Kahn, D., Nyaku, E., Li, J., Davis, S., and Jia, Y.: Ten Year Ozone Profile Record From Suomi NPP OMPS Limb Profiler, National Oceanic and Atmospheric Administration Washington D.C., District of Columbia, United States, Technical Review NASA Peer Committee 21 December 2022, [https://ntrs.nasa.gov/api/citations/20220019184/downloads/Fall\\_Meeting\\_2022\\_Kramarova\\_v3.pdf](https://ntrs.nasa.gov/api/citations/20220019184/downloads/Fall_Meeting_2022_Kramarova_v3.pdf) (last access: 9 March 2025), 2022.
- Kramarova, N. A., Xu, P., Mok, J., Bhartia, P. K., Jaross, G., Moy, L., Chen, Z., Frith, S., DeLand, M., Kahn, D., Labow, G., Li, J., Nyaku, E., Weaver, C., Ziemke, J., Davis, S., and Jia, Y.: Decade-long Ozone Profile Record from Suomi NPP OMPS Limb Profiler: Assessment of Version 2.6 Data, *Earth Space Sci.*, 11, e2024EA003707, <https://doi.org/10.1029/2024EA003707>, 2024.
- Li, F., Newman, P. A., and Waugh, D. W.: Impacts of stratospheric ozone recovery on southern ocean temperature and heat budget, *Geophys. Res. Lett.*, 50, e2023GL103951, <https://doi.org/10.1029/2023GL103951>, 2023a.

- Li, Z., Bi, J., Hu, Z., Ma, J., and Li, B.: Regional transportation and influence of atmospheric aerosols triggered by Tonga volcanic eruption, *Environ. Pollut.*, 325, 121429, <https://doi.org/10.1016/j.envpol.2023.121429>, 2023b.
- Livesey, N. J., Read, W. G., Wagner, P. A., Froidevaux, L., Santee, M. L., Schwartz, M. J., Lambert, A., Millán Valle, L. F., Pumphrey, H. C., Manney, G. L., Fuller, R. A., Jarnot, R. F., Knosp, B. W., and Lay, R. R.: Version 5.0x Level 2 and 3 data quality and description document, [https://mls.jpl.nasa.gov/data/v5-0\\_data\\_quality\\_document.pdf](https://mls.jpl.nasa.gov/data/v5-0_data_quality_document.pdf) (last access: 10 June 2025), 2022.
- Llewellyn, E. J., Lloyd, N. D., Degenstein, D. A., Gattinger, R. L., Petelina, S. V., Bourassa, A. E., Wiensz, J. T., Ivanov, E. V., McDade, I. C., Solheim, B. H., McConnell, J. C., Halev, C. S., von Savigny, C., Sioris, C. E., McLinden, C. A., Griffioen, E., Kaminski, J., Evans, W. F. J., Puckrin, E., Strong, K., Wehrle, V., Hum, R. H., Kendall, D. J. W., Matsushita, J., Murtagh, D. P., Brohede, S., Stegman, J., Witt, G., Barnes, G., Payne, W. F., Piché, L., Smith, K., Warshaw, G., Deslauniers, D.-L., Marchand, P., Richardson, E. H., King, R. A., Wevers, I., McCreath, W., Kyrölä, E., Oikarinen, L., Leppelmeier, G. W., Auvinen, H., Mégie, G., Hauchecorne, A., Lefèvre, F., de La Nöe, J., Ricaud, P., Frisk, U., Sjöberg, F., von Schéele, F., and Nordh, L.: The OSIRIS Instrument on the Odin Spacecraft, *Can. J. Phys.*, 82, 411–422, <https://doi.org/10.1139/p04-005>, 2004.
- Moy, L., Bhartia, P. K., Jaross, G., Loughman, R., Kramarova, N., Chen, Z., Taha, G., Chen, G., and Xu, P.: Altitude registration of limb-scattered radiation, *Atmos. Meas. Tech.*, 10, 167–178, <https://doi.org/10.5194/amt-10-167-2017>, 2017.
- NASA: OMPS data, available at: <https://disc.gsfc.nasa.gov/datasets> (last access: February 2025), 2025a.
- NASA: SHADOZ data, <https://tropo.gsfc.nasa.gov/shadoz/Archive.html> (last access: March 2025), 2025b.
- Qian, Y. Y., Luo, Y. H., Zhou, H. J., Yang, T. P., Xi, L., and Si, F. Q.: First Retrieval of Total Ozone Columns from EMI-2 Using the DOAS Method, *Remote Sens.*, 16, 1234–1245, <https://doi.org/10.3390/rs15061665>, 2024.
- Rault, D. F. and Loughman, R. P.: The OMPS Limb Profiler Environmental Data Record Algorithm Theoretical Basis Document and Expected Performance, *Ieee T. Geosci. Remote Sens.*, 51, 2505–2527, <https://doi.org/10.1109/TGRS.2012.2213093>, 2013.
- Rodgers, C. D.: Inverse methods for atmospheric sounding: theory and practice. Vol. 2. World scientific, 2000.
- Roth, C. Z., Degenstein, D. A., Bourassa, A. E., and Llewellyn, E. J.: The retrieval of vertical profiles of the ozone number density using Chappuis band absorption information and a multiplicative algebraic reconstruction technique, *Can. J. Phys.*, 85, 1225–1243, <https://doi.org/10.1139/p07-130>, 2007.
- Roazanov, V. V., Dinter, T., Roazanov, A. V., Wolanin, A., Bracher, A., and Burrows J.P.: Radiative transfer modeling through terrestrial atmosphere and ocean accounting for inelastic processes: Software package SCIATRAN, *J. Quant. Spectrosc. Ra.*, 194, 65–85, <https://doi.org/10.1016/j.jqsrt.2017.03.009>, 2017.
- Schwartz, M., Froidevaux, L., Livesey, N., and Read, W.: MLS/Aura Level 2 Ozone (O<sub>3</sub>) Mixing Ratio V005, Greenbelt, MD, USA, Goddard Earth Sciences Data and Information Services Center (GES DISC) [data set], <https://doi.org/10.5067/Aura/MLS/DATA2516>, 2020.
- Thompson, A. M., Witte, J. C., Smit, H. G., Oltmans, S. J., Johnson, B. J., Kirchhoff, V. W., and Schmidlin, F. J.: Southern Hemisphere Additional Ozonesondes (SHADOZ) 1998–2004 tropical ozone climatology: 3. Instrumentation, station-to-station variability, and evaluation with simulated flight profiles, *J. Geophys. Res.-Atmos.*, 112, <https://doi.org/10.1029/2005JD007042>, 2007.
- University of Saskatchewan: OSIRIS data, University of Saskatchewan, <https://research-groups.usask.ca/osiris/data-products.php> (last access: 25 July 2025), 2025.
- User's Guide for the software package SCIATRAN: Radiative Transfer Model and Retrieval Algorithm, Version 3.8, Institute of Remote Sensing, University of Bremen, Germany, February 9, 2018.
- Veefkind, J. P., de Haan, J. R., Brinksma, E. J., Kroon, M., and Levelt, P. F.: Total ozone from the Ozone Monitoring Instrument (OMI) using the DOAS technique, *Ieee T. Geosci. Remote Sens.*, 44, 1239–1244, <https://doi.org/10.1109/TGRS.2006.871204>, 2006.
- von Clarmann, T., Degenstein, D. A., Livesey, N. J., Bender, S., Braverman, A., Butz, A., Compernelle, S., Damadeo, R., Dueck, S., Eriksson, P., Funke, B., Johnson, M. C., Kasai, Y., Kepens, A., Kleinert, A., Kramarova, N. A., Laeng, A., Lange-rock, B., Payne, V. H., Roazanov, A., Sato, T. O., Schneider, M., Sheese, P., Sofieva, V., Stiller, G. P., von Savigny, C., and Zawada, D.: Overview: Estimating and reporting uncertainties in remotely sensed atmospheric composition and temperature, *Atmos. Meas. Tech.*, 13, 4393–4436, <https://doi.org/10.5194/amt-13-4393-2020>, 2020.
- Waters, J.W., Froidevaux, L., Harwood, R. S., Jarnot, R. F., Pickett, H. M., and Read, W. G.: The Earth Observing System Microwave Limb Sounder (EOS MLS) on the Aura satellite, *Ieee T. Geosci. Remote Sens.*, 44, 1075–1092, <https://doi.org/10.1109/TGRS.2006.873771>, 2006.
- Xu, P. Q., Bhartia, P. K., Jaross, G. R., DeLand, M. T., Larsen, J. C., Fleig, A., Kahn, D., Zhu, T., Chen, Z., Gorkavyi, N., Warner, J., Linda, M., Chen, H. G., Kowitt, M., Haken, M., and Hall, P.: Release 2 data products from the Ozone Mapping and Profiling Suite (OMPS) Limb Profiler, *Proc. SPIE 9242, Remote Sensing of Clouds and the Atmosphere XIX, and Optics in Atmospheric Propagation and Adaptive Systems XVII, 92420K (17 October 2014)*, <https://doi.org/10.1117/12.2067320>, 2014.
- Young, P. J., Harper, A. B., Huntingford, C., Paul, N. D., Morgenstern, O., Newman, P. A., Oman, L. D., Madronich, S., and Garcia, R. R.: The Montreal Protocol protects the terrestrial carbon sink, *Nature*, 596, 384–388, <https://doi.org/10.1038/s41586-021-03737-3>, 2021.
- Zawada, D. J., Rieger, L. A., Bourassa, A. E., and Degenstein, D. A.: Tomographic retrievals of ozone with the OMPS Limb Profiler: algorithm description and preliminary results, *Atmos. Meas. Tech.*, 11, 2375–2393, <https://doi.org/10.5194/amt-11-2375-2018>, 2018.
- Zhu, F., Si, F. Q., Zhan, K., Dou, K., and Zhou, H. J.: Inversion of Ozone Profile of Limb Radiation in Chappuis-Wulf Band, *Acta Opt. Sin.*, 41, 39–48, <https://doi.org/10.3788/AOS241244>, 2021.
- Zhu, F., Si, F. Q., Zhou, H. J., Dou, K., Zhao, M. J., and Zhang, Q.: Sensitivity Analysis of Ozone Profiles Retrieved from SCIAMACHY Limb Radiance Based on the Weighted Multiplicative Algebraic Reconstruction Technique, *Remote Sens.*, 14, 3954, <https://doi.org/10.3390/rs14163954>, 2022.

Zhu, F., Li, S.W., Yang, T. P., and Si, F. Q.: Research on Inversion and Application of Ozone Profile Based on OMPS Limb Scattering Observation, *Acta Opt. Sin.*, 45, 82–92, <https://doi.org/10.3788/AOS202141.0401005>, 2025a.

Zhu, F., Li, S. W., and Si, F. Q.: Retrieval of Ozone Profiles from Limb Scattering Measurements of the OMS on FY-3FSatellite, *Remote Sens.*, 17, 3784, <https://doi.org/10.3390/rs17233784>, 2025b.